Pedro Yuste, Juan M. Rius, Jordi Romeu, Sebastián Blanch,
Alexander Heldring, and Eduard Ubeda

A Microwave Invisibility Cloak

The design, simulation, and measurement of a simple and effective frequency-selective surface-based mantle cloak.

<AU: Please check whether the edited title and added subtitle are acceptable.>

xxxxxx

In recent years, there has been a growing interest in developing invisibility cloaks that can conceal an object. These techniques are often based either on coating a dielectric or conducting object with a homogeneous plasmonic layer of negative permittivity [1] or on a creating multilayer structure [2] that cancels the scattering of the cloaked object (i.e., scattering cancelation technique). **<AU: Please check whether the preceding edited sentence conveys the intended meaning.>** The technique may also be based on an inhomogeneous layer that bends electromagnetic waves around the region occupied by the cloaked object without interacting with it (i.e., transformation optics technique) [3].

Plasmonic- and transformation-based cloaks require materials of constituent properties not found in nature. The use of metamaterials made of lattices of subwavelength details [4], [5] achieves nonphysical values of dielectric permittivity and magnetic permeability, allowing the practical implementation of such cloaks in the microwave frequency band that is of interest here [6], [7].

An alternate approach is to optimize the cloak parameters to minimize scattering [8]–[11]. When the coating consists only of isotropic nonmagnetic dielectrics, the graded refraction index is physically realizable by varying doping profiles or nanoperforation [9], [10]. Transformation-based and plasmonic cloaks have important handicaps, such as bulky metamaterial layers, narrow bandwidth, sensitivity, and difficult implementation of the inhomogeneous refraction index profile or the negative constitutive parameters. The use of a frequency-selective surface (FSS) [12] as a mantle coat to achieve scattering cancelation [13], [14] allows for the easy building of a cloak for electrically thin cylinders using a simple, ultrathin, patterned conducting surface with important practical advantages, such as having a low profile, being lightweight, and having a broader band of operation. An excellent review of cloaking history and a summary of the scattering cancelation technique for both plasmonic and mantle cloaks can be found in [15].

Reducing forward scattering from electrically thin cylinders was first addressed by Kildal in the 1990s [16] by using the concept of hard and soft surfaces [17]. The topic is still under active research, using either hard surfaces [18] or FSS mantle cloaks [19]–[21]. **<AU: Please check whether the preceding edited sentence conveys the intended meaning.>** Recent advances include the ability to cloak the cylinder at both polarizations [22] using anisotropic FSS [23].

An FSS is probably the most cost-effective and easiest-to-implement choice for putting scattering cancelation into practice. The electromagnetic behavior of an FSS can be described

Digital Object Identifier 10.1109/MAP.2018.2839903
Date of publication: xxxxxx

by means of surface impedance; hence, Z_s, which relates the averaged tangential electric field on the surface to the averaged induced electric current density:

$$\boldsymbol{E}_t = Z_s \cdot \boldsymbol{J}_s, \tag{1}$$

$$\hat{\boldsymbol{n}} \times (\boldsymbol{H}^{\text{out}} - \boldsymbol{H}^{\text{in}}) = \boldsymbol{J}_s, \tag{2}$$

where $\boldsymbol{H}^{\text{out}}$ is the magnetic field in the outer face of the FSS and $\boldsymbol{H}^{\text{in}}$ is the magnetic field in the inner face. The average surface impedance Z_s is ideally assumed uniform along the metasurface.

The geometry of an FSS cloak, consisting of a very thin metallic layer, can be designed to implement the average surface impedance that minimizes the scattered field. Moreover, at microwave frequencies, the FSS can be assumed lossless; thus, its average surface impedance is purely reactive, $Z_s = jX_s$, if the power dissipated at the FSS is zero:

$$\begin{aligned} P^{\text{out}} - P^{\text{in}} &= \Re[\boldsymbol{E}_t \times (\boldsymbol{H}_t^{\text{out}} - \boldsymbol{H}_t^{\text{in}})^*] \\ &= \Re[Z_s |\boldsymbol{H}_t^{\text{out}} - \boldsymbol{H}_t^{\text{in}}|^2] = 0. \end{aligned} \tag{3}$$

Although the scattering cancelation technique and the design of FSS mantle cloaks have been fully addressed in the literature, the complete presentation of theory development, design procedure, simulation techniques, prototype building, and measurement results is scattered among many books and articles, leading the novice practitioner to leap from one source to another to get the overall picture. The aim of this article is to didactically present the complete process, letting readers reproduce it and easily build a simple and inexpensive cloak like that of [19]. In particular, the derivation of the scattering coefficients in (15) is fully developed in the section "Mantle Cloaking Fundamentals" because it cannot be found in the references cited here or in the references cited by the literature. **<AU: Please check whether the preceding edited sentence conveys the intended meaning.>** Although some books derive the scattering coefficients for bare dielectric cylinders, we have not found the derivation given here for the coated case.

MANTLE CLOAKING FUNDAMENTALS

Consider the scenario presented in Figure 1. A circular cylinder of radius a, dielectric permittivity equal to ε_1, and magnetic permeability equal to μ_1 was coated with a zero-thickness surface of impedance Z_s (i.e., the cloak), located at $\rho = a$. For practical purposes, we consider a nonmagnetic cylinder of $\mu_1 = \mu_0$. The value of the coat surface impedance Z_s was designed to achieve cancelation between the scattering from the bare dielectric cylinder and that from the coat.

Let us assume a TMz-polarized **<AU: Kindly spell out TMz.>** impinging plane wave propagating along the x axis,

$$\boldsymbol{E}^i = \hat{\boldsymbol{z}} E_0 e^{-jk_0 x} = \hat{\boldsymbol{z}} E_0 e^{-jk_0 \rho \cos\phi}, \tag{4}$$

where e^{jwt} harmonic time variation is assumed. According to the Jacobi-Anger expansion, the plane wave can be expressed in terms of cylindrical harmonics as [25]

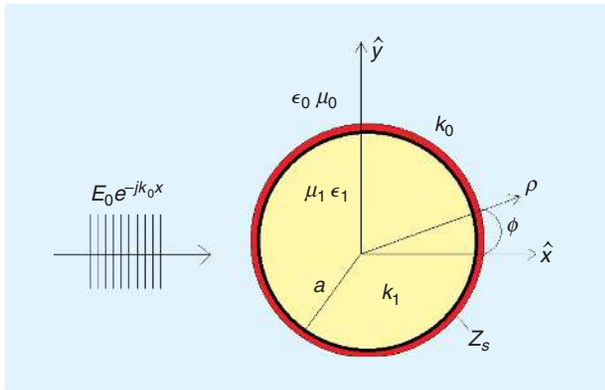

FIGURE 1. A geometrical layout of the dielectric cylinder (in yellow) and the cloak (in red).

$$\boldsymbol{E}^i = \hat{\boldsymbol{z}} E_0 \sum_{n=-\infty}^{\infty} j^{-n} J_n(k_0\rho) e^{jn\phi}. \tag{5}$$

Similarly, the cylindrical wave expansion for the scattered electric field outside the dielectric cylinder is

$$\boldsymbol{E}^s = E_z^s \hat{\boldsymbol{z}} = \hat{\boldsymbol{z}} E_0 \sum_{n=-\infty}^{\infty} a_n H_n^{(2)}(k_0\rho) e^{jn\phi}, \tag{6}$$

where a_n is the scattering coefficient and $H_n^{(2)}$ is the Hankel function of the second kind [25] that represents outward traveling cylindrical waves.

The total electric field inside the cylinder is expanded in cylindrical harmonics as

$$\boldsymbol{E}^{\text{in}} = \hat{\boldsymbol{z}} E_0 \sum_{n=-\infty}^{\infty} b_n J_n(k_1\rho) e^{jn\phi}, \tag{7}$$

where b_n is the coefficient of the cylindrical modes inside the dielectric. Outside the cylinder, the total field is

$$\boldsymbol{E}^{\text{out}} = \boldsymbol{E}^s + \boldsymbol{E}^i. \tag{8}$$

The magnetic-field boundary condition at the coating layer, $\rho = a$, for the layout of Figure 1 is

$$\hat{\boldsymbol{n}} \times (H_\phi^{\text{out}} - H_\phi^{\text{in}})\hat{\boldsymbol{\phi}}\big|_{\rho=a} = J_z \hat{\boldsymbol{z}}\big|_{\rho=a} = \frac{E_z}{Z_s}\hat{\boldsymbol{z}}\Big|_{\rho=a}, \tag{9}$$

where Z_s is the coat surface impedance and $\hat{n}$ the unit normal to the surface.

The magnetic field inside and outside the cylinder was obtained from the electric field (7) and (8) after applying Maxwell-Faraday curl equation:

- magnetic field inside ($\rho < a$):

$$H_\phi^{\text{in}} = \frac{1}{jk_1\eta_1} \sum_{n=-\infty}^{\infty} b_n k_1 J_n'(k_1\rho) e^{jn\phi}, \tag{10}$$

- magnetic field outside ($\rho > a$):

$$\begin{aligned} H_\phi^{\text{out}} = \frac{1}{jk_0\eta_0} \sum_{n=-\infty}^{\infty} [&j^{-n} k_0 J_n'(k_0\rho) + \\ &+ a_n k_0 H_n'^{(2)}(k_0\rho)] e^{jn\phi}, \end{aligned} \tag{11}$$

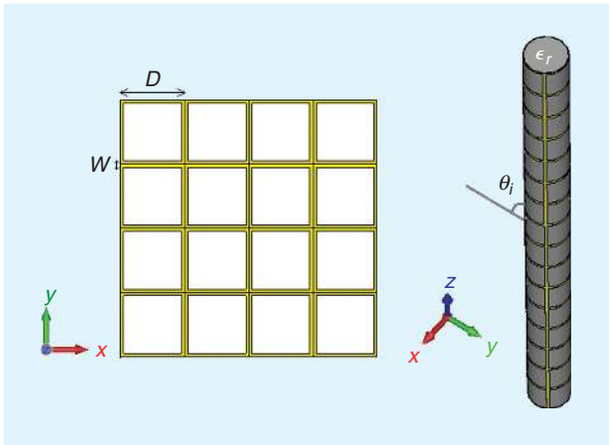

FIGURE 2. The mesh-grid FSS geometry. ***<AU: From where was this image obtained, and do you have permission from the source to use it?>***

where the prime symbol denotes the derivative with respect to the argument of Bessel functions [25].

Since (9) states that $E_z = Z_s(H_\phi^{\text{out}} - H_\phi^{\text{in}})$ at $\rho = a$,

$$E_z = \sum_{n=-\infty}^{\infty} \left[\frac{1}{jk_0\eta_0}(Z_s j^{-n} k_0 J_n'(k_0 a) + a_n Z_s k_0 H_n'^{(2)}(k_0 a)) - \frac{1}{jk_1\eta_1}(b_n Z_s k_1 J_n'(k_1 a)) \right] e^{jn\phi}. \quad (12)$$

According to the boundary condition for the electric field $(E_z^{\text{out}} - E_z^{\text{in}})|_{\rho=a} = 0$ and using (8) together with the cylindrical mode expansions (6) and (7),

$$E_z = \sum_{n=-\infty}^{\infty} [j^{-n} J_n(k_0 a) + a_n H_n^{(2)}(k_0 a)] e^{jn\phi} = \sum_{n=-\infty}^{\infty} b_n J_n(k_1 a) e^{jn\phi}. \quad (13)$$

The combination of (12) and (13) easily leads to the following system of equations:

$$\begin{pmatrix} H_n^{(2)}(k_0 a) & -J_n(k_1 a) \\ \frac{1}{j\eta_0} Z_s H_n^{(2)'}(k_0 a) & -\frac{1}{j\eta_1} Z_s J_n'(k_1 a) - J_n(k_1 a) \end{pmatrix} \begin{pmatrix} a_n \\ b_n \end{pmatrix} = \begin{pmatrix} -j^{-n} J_n(k_0 a) \\ -j^{-n} \frac{1}{j\eta_0} Z_s J_n'(k_0 a) \end{pmatrix}. \quad (14)$$

The solution for the scattering coefficients a_n using Cramer's rule is

$$a_n = \frac{j^{-n} \begin{vmatrix} J_n(k_0 a) & J_n(k_1 a) \\ Z_s J_n'(k_0 a) & n_1 Z_s J_n'(k_1 a) - j\eta_0 J_n(k_1 a) \end{vmatrix}}{\begin{vmatrix} H_n^{(2)}(k_0 a) & -J_n(k_1 a) \\ Z_s H_n'^{(2)}(k_0 a) & -n_1 Z_s J_n'(k_1 a) - j\eta_0 J_n(k_1 a) \end{vmatrix}}, \quad (15)$$

where $n_1 = (\eta_0/\eta_1) = \sqrt{(\varepsilon_1/\varepsilon_0)}$.

Because we have only one degree of freedom, Z_s, only a single cylindrical harmonic of the scattered field can be zeroed to minimize scattering. If the cylinder is electrically thin, $a \ll \lambda$, the dominant harmonic is the lowest order, and, therefore, we design Z_s to achieve $a_0 = 0$:

$$Z_s = jX_s = j\frac{\eta_0 J_0(k_0 a) J_0(k_1 a)}{n_1 J_0(k_0 a) J_1(k_1 a) - J_1(k_0 a) J_0(k_1 a)}, \quad (16)$$

where we have used the identity $J_0'(ka) = -J_1(ka)$ [25] to remove the derivatives. For electrically wider cylinders, $a_0 \sim \lambda$, we could consider minimizing the square sum of the lowest-order coefficients $|a_0|^2 + |a_1|^2 + \ldots$ instead of forcing $a_0 = 0$.

This result gave the surface reactance of the cloaking coat attached to an electrically thin cylinder that minimized the scattered field and, thus, reduced its visibility. The polyvinyl chloride (PVC) cylinder to coat here had dielectric permittivity $\varepsilon_r = 2.723$, measured with the waveguide method [26], and a radius $a = 1.34$ cm. At the design frequency of 3.77 GHz, the required coat impedance was $Z_s = j192.5\ \Omega$.

The coat was implemented with an FSS [12]. One of the simplest and easiest-to-build FSS designs is the mesh grid shown in Figure 2. For this metasurface, the equivalent surface impedance Z_s depended on geometrical dimensions as follows, for the TM-polarized **<AU: Kindly spell out TM.>** case [27]:

$$Z_s^{TM} = j\eta_0 \frac{D}{\lambda} \ln\left(\csc\left(\frac{\pi w}{4D}\right)\right)\left(1 - \frac{\sin^2\theta_s}{\varepsilon_r + 1}\right), \quad (17)$$

where D is the mesh period, w the strip width, $c = 3 \cdot 10^8$ m/s, and θ_s is the angle of incidence. **<AU: Kindly check that the preceding edited sentence conveys the intended meaning.>**

To obtain a surface reactance of 192.5 Ω at 3.77 GHz for normal incidence $\theta_s = \pi/2$, the period and strip width of the mesh-grid FSS cells are $D = 2.1$ cm and $w = 1.9$ mm, respectively.

NUMERICAL SIMULATION

The simulation model is a replica of the PVC cylinder to be cloaked and measured, but it is shorter in length. It was a 33.6-cm-long circular cylinder with radius $a = 1.34$ cm. Relative permittivity of the dielectric material (i.e., PVC) was experimentally measured with the waveguide method and found to be $\varepsilon_r = 2.723$.

The incoming TMz-polarized plane wave impinged perpendicularly to the cylinder axis, oriented parallel to the z-axis, with the angle of incidence $\theta_i = (\pi/2)$. The FSS mesh-grid dimensions (Figure 2) were $D = 2.1$ cm and $w = 1.9$ mm. The copper grid was modeled as an infinitely thin surface of conductivity equal to $60 \cdot 10^6 \Omega^{-1} m^{-1}$. The dielectric cylinder and coat model was centered at the coordinate origin.

The cloak metasurface was meshed into RWG **<AU: Kindly spell out RWG.>** basis functions [28] (Figure 3) and the dielectric cylinder into pairs of tetrahedrons [29]. The problem was modeled with the surface-volume [30] electric field integral equation [31] and discretized by the method of moments [32]. The numerical code used was called *fast integral equation solver for scatterers and antennas in three dimensions* (*FIESTA-3-D*) [33], a software package developed at the AntennaLab of the Universitat Politècnica de Catalunya.

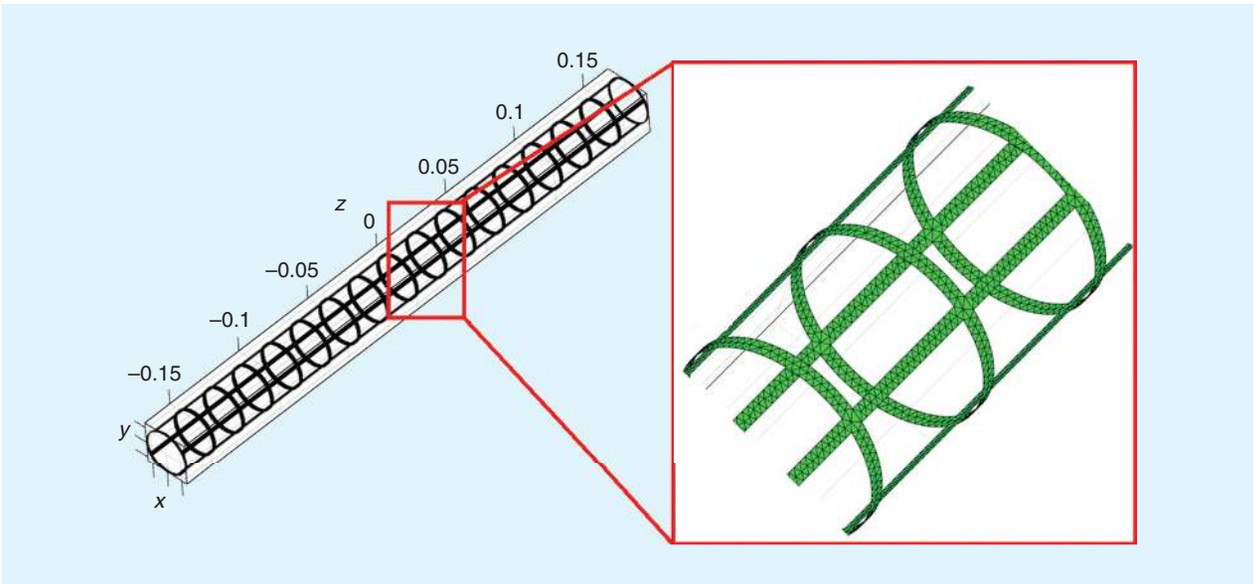

FIGURE 3. The mesh-grid FSS structure and a zoomed view of the triangle mesh. ***<AU: From where was this image obtained, and do you have permission from the source to use it?>***

FSS IMPEDENCE

After full-wave computation of the field scattered by the cloaked three-dimensional (3-D) cylinder along a circle of radius ρ in the xy plane and centered at the origin, $E^s_{z3D}(\phi)$, we obtained the zeroth-order scattering coefficient a_0 and the cloak surface impedance as follows.

Since a_0 is the coefficient of the lowest-order cylindrical harmonic of the two-dimensional (2-D) field scattered by the infinite cylinder, E^s_{TM2D}, we first had to use the approximate relation

$$E^s_{TM2D} \approx E^s_{z3D} \frac{\sqrt{\lambda\rho}}{Le^{j\frac{\pi}{4}}} \tag{18}$$

to estimate the 2-D scattering of the infinite cylinder from the 3-D computation for a finite cylinder of length L. Equation (18) is valid in the far field for electrically long cylinders, with $L \gg \lambda$, and normal plane-wave incidence polarized parallel to the cylinder axis [34]. This relation can be easily derived by comparing the 2-D scattered field

$$E^s_{TM2D} = -jk\eta \int_C J_{z2D}(\boldsymbol{\rho}') \frac{H_0^{(2)}(KR)}{4j} d\boldsymbol{\rho}', \quad R = |\boldsymbol{\rho} - \boldsymbol{\rho}'| \tag{19}$$

with the 3-D case

$$E^s_{z3D} = -jk\eta \int_{-L/2}^{L/2} \int_C J_{z3D}(\boldsymbol{r}') \frac{e^{-jKR}}{4\pi R} d\boldsymbol{r}', \quad R = |\boldsymbol{r} - \boldsymbol{r}'| \tag{20}$$

for $\boldsymbol{r} = \boldsymbol{\rho}$ (observer in the xy plane), after using the large argument approximation for $H_0^{(2)}$ [see (23)] and the parallel ray approximation $e^{-jkR} \approx e^{-jkr} e^{jk\hat{\boldsymbol{r}}\cdot\boldsymbol{r}'}$.

Notice that the main approximation here assumes that the induced current in the 3-D case is z-directed, uniform along the z-direction, and the same as in 2-D:

$$\boldsymbol{J}_{3D}(\boldsymbol{r}') \approx J_{z3D}(\boldsymbol{\rho}')\hat{\boldsymbol{z}} \approx J_{z2D}(\boldsymbol{\rho}')\hat{\boldsymbol{z}}. \tag{21}$$

This assumption will be valid if the edge effects can be neglected, which needs $L \gg \lambda$.

The cylindrical harmonic coefficients of the 2-D scattered field of (6), a_n, were computed from the Fourier series coefficients of $E^s_{TM2D}(\phi) = E^s_z(\phi)$ as

$$a_n = \frac{1}{2\pi H_n^{(2)}(k_0\rho)} \int_0^{2\pi} E^s_z(\rho,\phi) e^{-jn\phi} d\phi. \tag{22}$$

Using the large argument approximation of the second-kind Hankel function,

$$H_n^{(2)}(k_0\rho) \approx \sqrt{\frac{2}{\pi k_0\rho}} e^{-j(k_0\rho - n\frac{\pi}{2} - \frac{\pi}{4})}, \quad k_0\rho \to \infty, \tag{23}$$

and substituting (18) and (23) into (22) for $n = 0$ led to

$$a_0 = \frac{j}{2L} \int_0^{2\pi} E^s(\phi)\, d\phi. \tag{24}$$

Now, one can find the cylindrical FSS impedance of the cloak by isolating Zs in (15):

$$Z_s = \frac{j\eta_0 (a_0 H_{00} J_{01} + J_{00} J_{01})}{a_0 n_1 H_{00} J_{11} - a_0 H_{10} J_{01} + n_1 J_{00} J_{11} - J_{01} J_{10}}, \tag{25}$$

where

$$J_{00} = J_0(k_0 a) \qquad J_{01} = J_0(k_1 a),$$
$$J_{10} = J_1(k_0 a) \qquad J_{11} = J_1(k_1 a),$$

and

$$H_{00} = H_0^{(2)}(k_0 a) \qquad H_{10} = H_1^{(2)}(k_0 a).$$

Figure 4 shows the evolution of the surface impedance Z_s as a function of frequency. At the design frequency of 3.77 GHz, the reactance (i.e., the red line) was 190.0 Ω instead of the theoretical value of 192.5 Ω. As expected, the real part of the

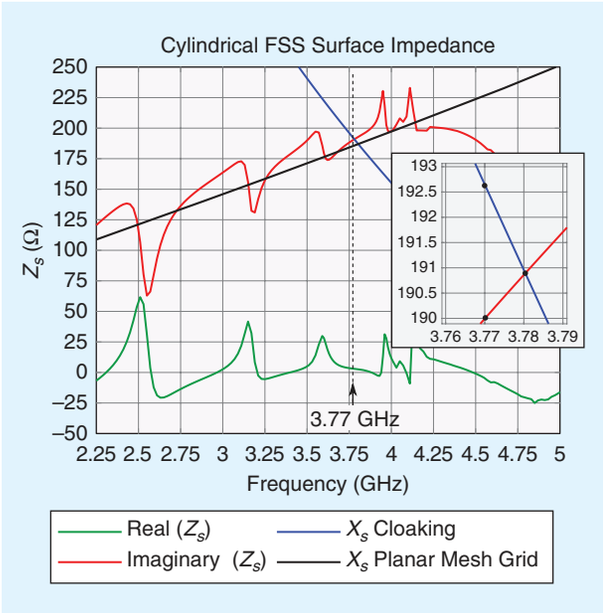

FIGURE 4. The simulated surface impedance of the cylindrical FSS as a function of frequency (real part R_s in green and imaginary part X_s in red), together with the reactance of the infinite planar mesh-grid FSS determined using computer-simulated technology software (in black) and the required reactance for ideal cloaking from (16) in blue. The cylindrical FSS reactance at the 3.77-GHz design frequency is 190.0 Ω instead of the theoretical value of 192.5 Ω and achieves the required reactance for ideal cloaking at a frequency of 3.78 GHz with an almost-zero resistance at that frequency.

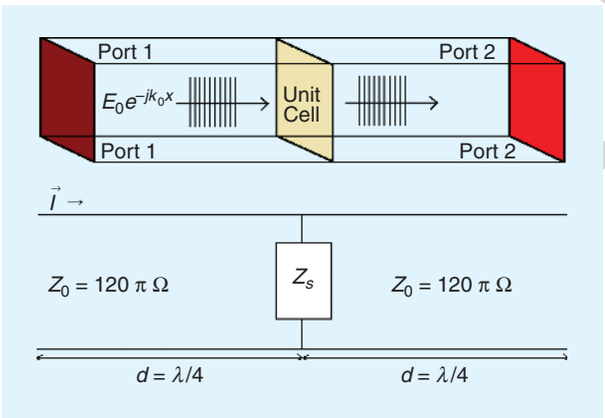

FIGURE 5. A transmission line model for an FSS of impedance Z_s and normal incident plane wave.

surface impedance was much smaller than the reactance (i.e., the green line).

It is interesting to compare the computed surface impedance for the cylindrical FSS with the required reactance for ideal cloaking from (16) (i.e., the blue line in Figure 4). The two lines cross each other at 3.78 GHz with an almost-zero resistance at that frequency. Therefore, the cloak is expected to work successfully at a frequency of 3.78 instead of 3.77 GHz.

We can also compare this with the surface impedance of the planar infinite mesh grid, for which (17), used to design the cell dimensions, is valid. Infinite planar periodic structures can be

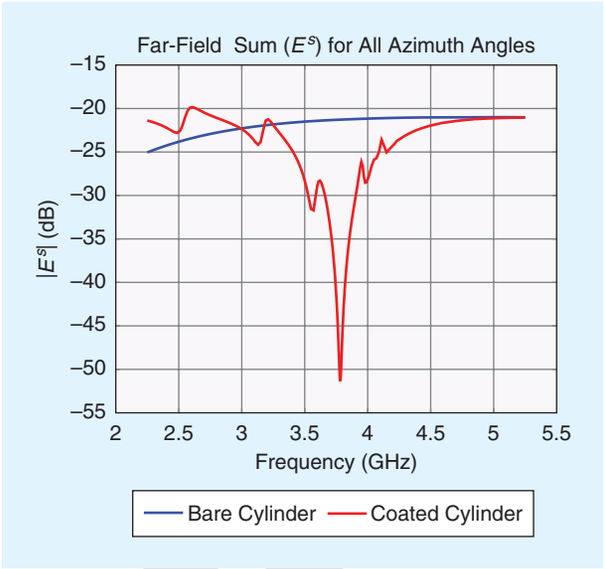

FIGURE 6. The integration of $E^s(\phi)$ for ϕ as a function of frequency for the bare dielectric cylinder (blue line) and the coated cylinder (red line).

easily analyzed using Floquet mode theory from the simulation of a single cell. Since Floquet modes were not implemented in the FIESTA-3-D code, computer simulation technology (CST) was used [35]. In the CST, two Floquet ports were placed at both sides of a mesh-grid cell and computed S-parameters. The FSS impedance, Z_s, was related to parameter S_{11} using the equivalent transmission line model of Figure 5:

$$Z_s = -Z_0\left(\frac{1 + S_{11\text{cell}}}{2S_{11\text{cell}}}\right), \tag{26}$$

where $S_{11\text{cell}} = S_{11\text{port}}\, e^{(j2\pi d/\lambda)}$, with d being the length of the transmission line from the Floquet port to the FSS plane and $S_{11\text{port}}$ being the reflection coefficient computed by CST at the ports. The black line in Figure 4 shows the reactance computed for the infinite planar mesh-grid FSS. The real part R_s is zero at all frequencies, since Z_s is purely reactive in the ideal case.

The planar FSS reactance at the design frequency (i.e., 184.9 Ω at 3.77 GHz) was very close to the value obtained by the full-wave 3-D simulation of the cylindrical FSS (i.e., 190.0 Ω). This suggests that the mesh-grid geometry was correctly designed and the bending of the FSS in a curved surface did not significantly change the surface impedance near 3.77 GHz.

There are frequencies at which the surface reactance of the cylindrical FSS departed from the value for the infinite planar mesh grid computed by CST, having a very significant real part that ideally should be zero. This behavior resembles a kind of resonance specific to the cylindrical case and suggests that there are frequencies at which the design of the cloak using (17), valid for the planar case, may not work as expected.

FULL-WAVE SIMULATION OF MANTLE CLOAKING

To assess cloaking performance, we simulated the bare dielectric cylinder and the cloaked one with FIESTA-3-D [33].

Figure 6 shows the integration of far fields $E^s(\phi)$ for ϕ angles around the cylinder, which, according to (22) and (24), is proportional to the dominant scattering coefficient a_0 that should ideally be null. Figure 7 shows the cloak attenuation computed by subtracting the two results of Figure 6: the red line is the FIESTA-3-D simulation result, while the blue line corresponds to the theoretical calculation of the 2-D cylindrical expansion coefficient a_0 with (15), using the ideal planar FSS impedance given by (17), which provides $a_0 = 0$ at the design frequency (i.e., 3.77 GHz).

The simulated cloaking effect was very good. The FIESTA-3-D full-wave simulation (i.e., the red line in Figure 7) gave almost a 30-dB scattering reduction and agreed well with the theoretical value of the 2-D scattering coefficient a_0. The cloaking frequency was slightly shifted from the design value (i.e., 3.77 GHz) to 3.78 GHz, exactly as was predicted from the computed reactance of the cylindrical FSS in Figure 4.

The cloaking performance can also be observed in the far-field pattern at the 3.77-GHz design frequency (Figure 8) in contrast with the noncloaking pattern at a far-away frequency (Figure 9). The cloaked-cylinder pattern of Figure 8 has the shape of the $n = 1$ cylindrical harmonic, after cancelation of the a_0 coefficient of the dominant zeroth-order mode. Since, in this case, $k_1 a = 1.75$ at 3.77 GHz, the first-order harmonic a_1 was not small enough, and we could have obtained a better result by minimizing $|a_0|^2 + |a_1|^2$.

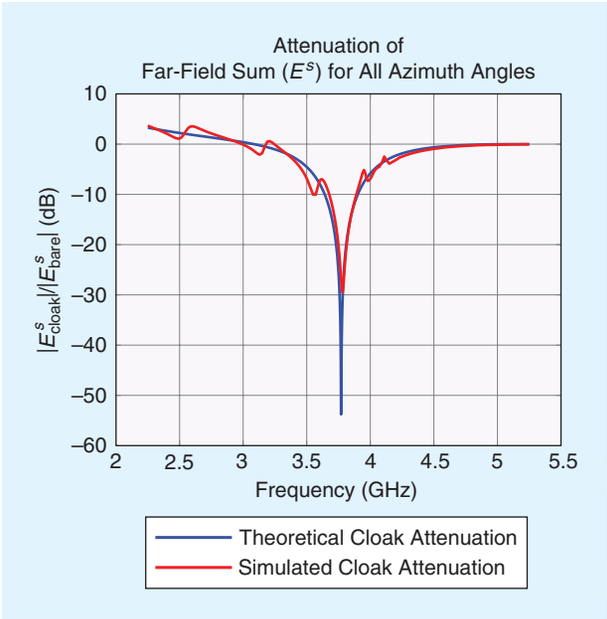

FIGURE 7. The cloaking attenuation of the scattered field, equal to the coated-cylinder field normalized with the bare-cylinder field, $E^s_{z\,\text{cloak}}/E^s_{z\,\text{bare}}$. The full-wave computation for a 3-D cylinder (red line) is compared to the theoretical calculation of the 2-D cylindrical harmonic a_0 coefficient (blue line).

MANUFACTURING AND EXPERIMENTAL TESTING

PROTOTYPE

The cloak prototype was a simple 32 × 4-cell cylindrical copper sheet, as depicted in Figures 2 and 3. The geometrical dimensions were the same as in the model simulated with FIESTA-3-D in the section "Numerical Simulation," except for the PVC cylinder length (1 m) and the cloak height (51 cm), and, thus, coated only the center part of the cylinder. Since the main lobe of the transmitting antenna impinged over only the coated part of the cylinder, the simulations for an incident plane wave, as discussed in the "Numerical Simulation" section, should have approximately predicted the measurement results.

The PVC cylinder was bought from Lumetal Plastic S.L. **<AU: Please spell out S.L., if appropriate.>** (http://www.

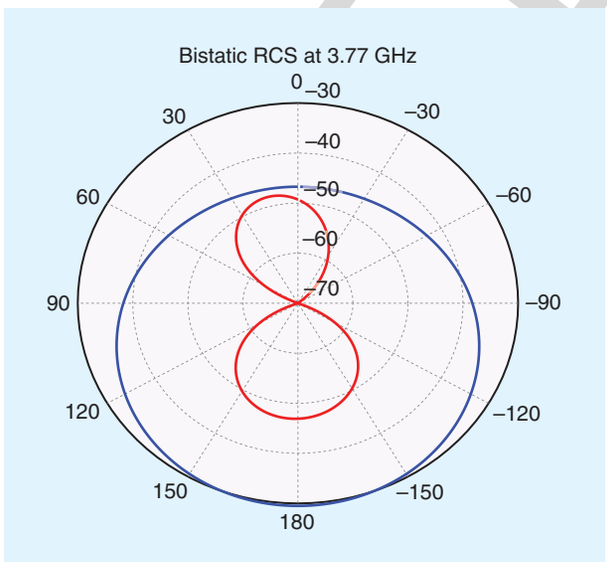

FIGURE 8. The bistatic RCS **<AU: Kindly spell out RCS.>** patterns for the bare (blue) and cloaked (red) cylinders at the 3.77 GHz design frequency.

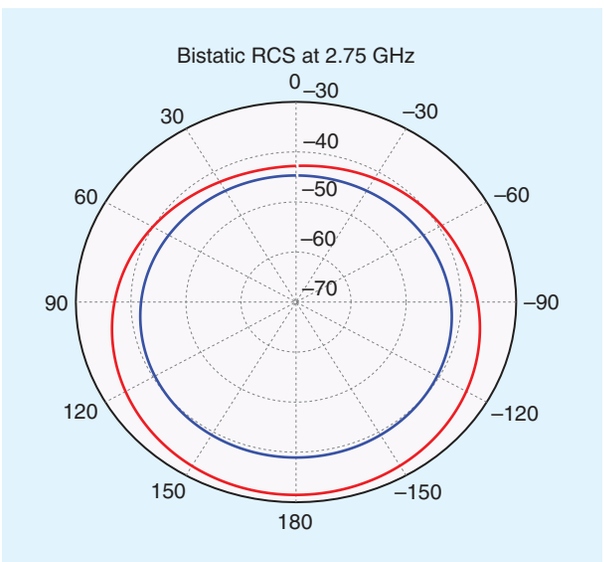

FIGURE 9. The bistatic RCS patterns for the bare (blue) and cloaked (red) cylinders at 2.75 GHz, far away from the design frequency.

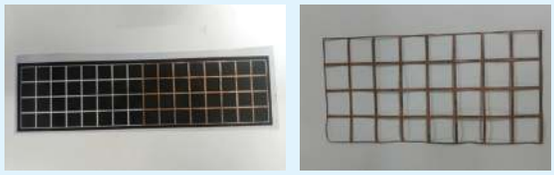

FIGURE 10. (a) A black-and-white plastic film mask, e.g., a negative image, was used to print the mesh-grid design on the copper sheet metal. (b) The final resulting 8 × 4-cell section of cloak. ***<AU: From where were these images obtained, and do you have permission from the source to use them?>***

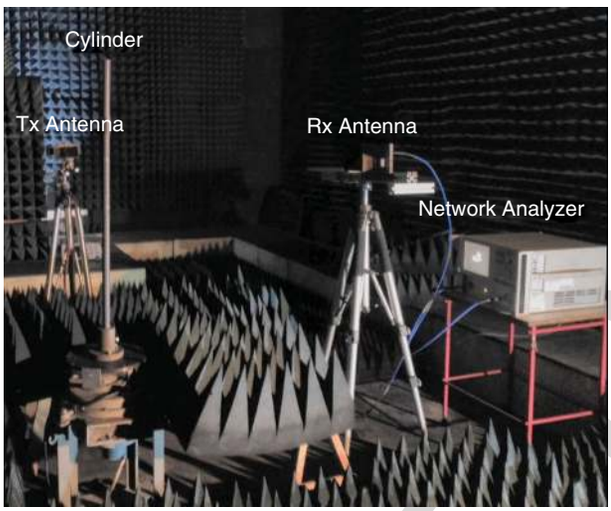

FIGURE 11. The bistatic scattering measurement setup at four different angles. Tx: Transmit; Rx: Receive. ***<AU: Kindly check that Tx and Rx are spelled out correctly. Also, from where was this image obtained, and do you have permission from the source to use it?>***

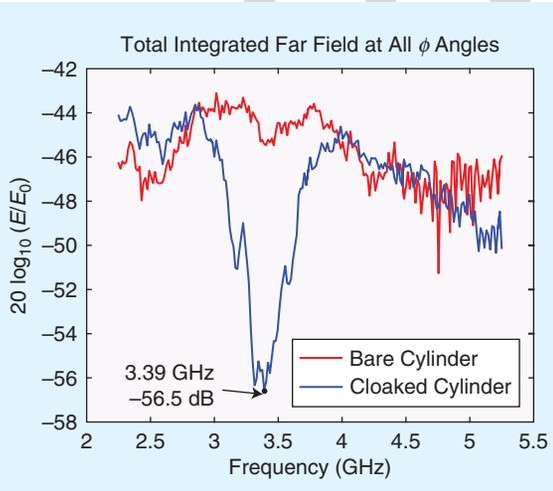

FIGURE 12. The measured electric field was integrated around the cylinder by the coherent sum of all the bistatic measurements. The scattered field was attenuated about 10 dB by the cloak in a frequency band around 3.39 GHz.

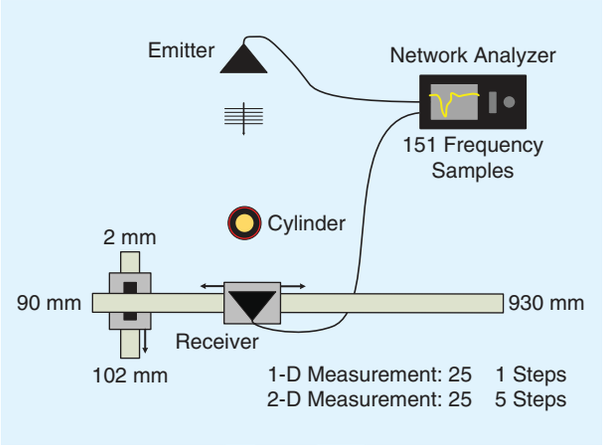

FIGURE 13. The forward near-field 2-D measurement setup with two stepping motors. 1-D: one dimensional. ***<AU: Kindly check that 1-D is spelled out correctly.>***

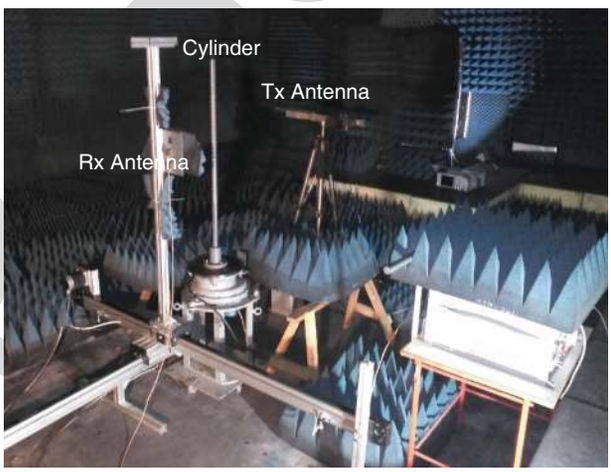

FIGURE 14. The forward near-field 2-D measurement setup. ***<AU: From where was this image obtained, and do you have permission from the source to use it?>***

lumetalplastic.com/en/) and used as is, with no modification. The copper sheet had a thickness of 70 μm, and it was patterned by a standard chemical photoetching process. First, the photoresist was deposited on the copper sheet, and the desired pattern was transferred through a film mask. The plastic film and the copper coat after the chemical process are shown in Figure 10. The full 32 × 4-cell sheet was assembled using four different 8 × 4 sections. Finally, the FSS structure was carefully glued to the surface of the dielectric cylinder. To achieve a very thin and uniform glue layer, 3-μ **<AU: Please check that the change of "M" to "μ" is correct.>** photo-mount glue was sprayed over the copper sheet, and the dielectric cylinder was rolled over the glue.

MEASUREMENT OF BISTATIC SCATTERING

The first set of measurements corresponded to the bistatic problem. The setup for the bistatic measurement is shown in Figure 11. The whole setup was placed in an anechoic chamber to avoid the effect of unwanted reflections. Two ridge-horn antennas

that cover the frequency range 2–15 GHz were mounted on tripods and connected to each of the ports of an automatic network analyzer. One of the antennas remained fixed, and the other was placed at 45°, 90°, 135°, and 180°. The S_{11} measurement provided the back-scattering at 0° and S_{12} at the remaining positions. Time-domain gating was applied to filter out the antenna reflection in the S_{11} measurements.

Figure 12 shows the coherent summation of the bistatic measurements obtained at different angular positions as a function of the operating frequency. Despite the simple cloak design, the scattering attenuation achieved by this prototype was approximately 10 dB. Noticeably, the attenuation peak was located at 3.4 GHz instead of the design frequency (i.e., 3.77 GHz). The most likely explanation for this discrepancy is the lack of manufacturing precision, since small inaccuracies lead to variations of the surface impedance that shift the cancelation frequency of the field scattered by the cloak with that of the dielectric cylinder. Although the technique was narrow-band in nature, a remarkable bandwidth of the order of 100 MHz was achieved.

MEASUREMENT OF NEAR-FIELD MAGNITUDE

A second set of measurements was carried out to measure the field distribution behind the cylinder. The goal of the measurements was to verify that the field distributions measured around the cloaked-cylinder prototype resembled those that would be measured without the presence of the cylinder. A ridge-horn antenna was used to produce the illuminating fields on the test zone. The measuring distance was chosen to be at least ten wavelengths away from the antenna to ensure plane-wave conditions on the cylinder. No specific level calibration was performed since only relative measurements were of interest, e.g., comparing the fields without the cylinder, with the cylinder, and with the cloaked cylinder.

Two stepping motors were used to measure the magnitude and phase of the forward near field in a 2-D grid. As shown in Figure 13, the emitter antenna remained static while the receiver was moved along five rows in the y-direction, measuring 25 field samples in each row in the x-direction. The anechoic chamber setup can be observed in Figure 14.

Figures 15 and 16 show the measurements in the 2-D grid of Figure 13 for, respectively, the frequency of minimum scattering (i.e., 3.39 GHz) and a frequency far away from the cloaking band (i.e., 2.75 GHz). The grid was located behind the cylinder in the forward near-field zone, at a minimum distance of approximately 50 cm from the cylinder surface, as shown in Figures 13 and 14.

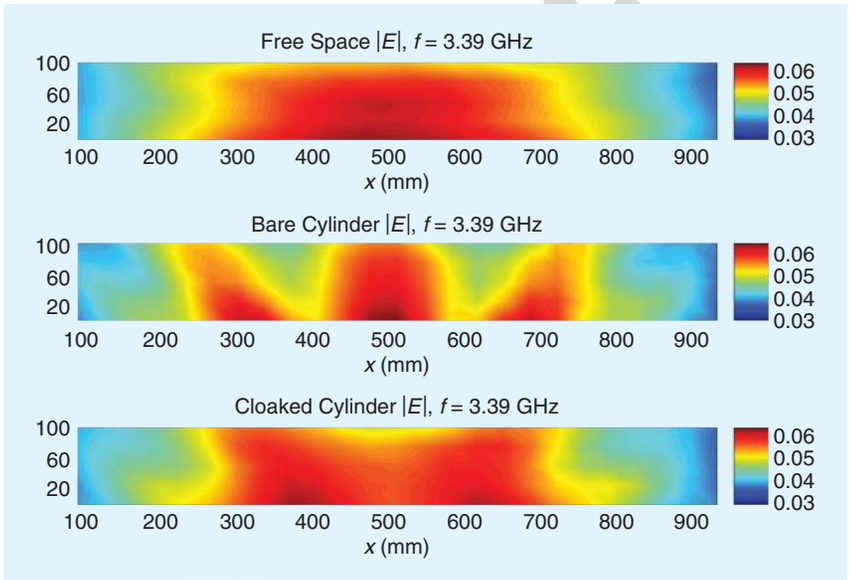

FIGURE 15. The 2-D measurement of forward-field magnitude for the free-space measurement (i.e., the incident field with no cylinder) and the bare dielectric and cloaked cylinder at the frequency of minimum scattering (i.e., 3.39 GHz). As expected, the cloak partly restores the incident-field distribution for operating frequencies in the cloaking band.

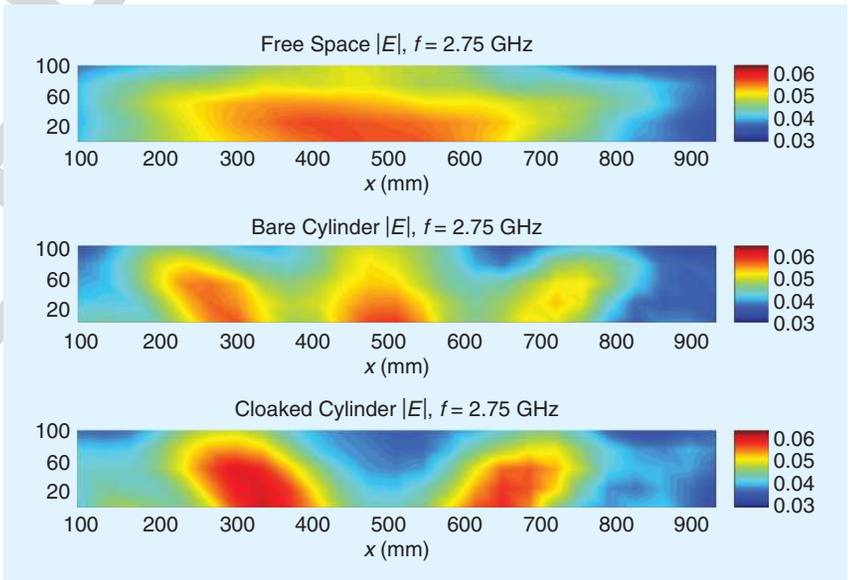

FIGURE 16. The 2-D measurement of forward-field magnitude for the free-space measurement (i.e., the incident field with no cylinder), the bare dielectric cylinder, and the cloaked one at a frequency far away from the cloaking band (2.75 GHz). At this frequency, there is no cloaking effect, and the incident field is heavily distorted by the presence of the bare or cloaked cylinder.

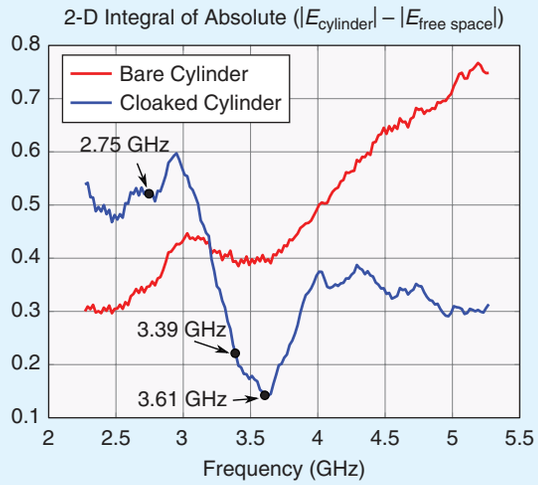

FIGURE 17. The absolute value of the difference between the free-space (i.e., incident) field and the cloaked-cylinder field magnitudes, integrated for all points into the 2-D near-field grid. The red and blue lines correspond to the difference between the free-space field and, respectively, the bare- or cloaked-cylinder fields. The black circles show the frequencies of 2.75 and 3.39 GHz, corresponding to the results in Figures 15 and 16, and the frequency for which the cloak best restores the incident field (i.e., 3.61 GHz), corresponding to Figure 18.

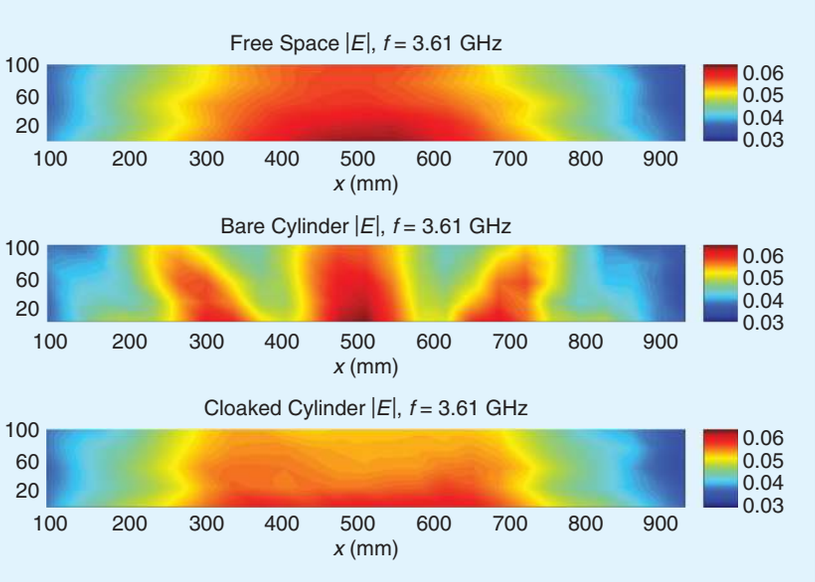

FIGURE 18. The 2-D measurement of forward-field magnitude for the free-space measurement (i.e., the incident field with no cylinder) and the bare dielectric and cloaked cylinder at the frequency of minimum difference between the free-space and the cloaked-cylinder near field (i.e., 3.61 GHz). The cloak partly restores the incident-field distribution.

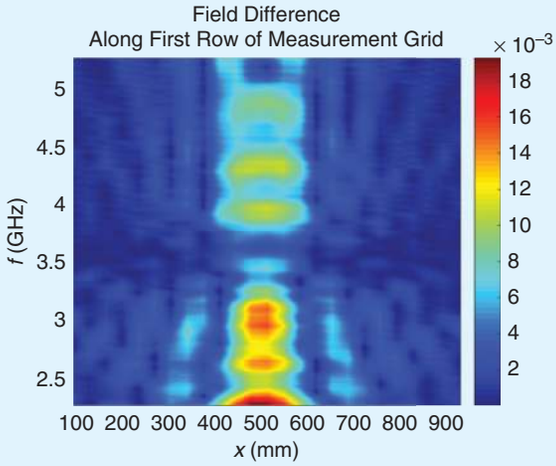

FIGURE 19. The absolute value of the difference between the free-space and the cloaked-cylinder field magnitudes along the first row (i.e., the *x*-direction) of the 2-D measurement grid versus the frequency. The cloaking band between 3.4 and 3.7 GHz—in which the incident and the cloaked-cylinder fields are similar so that the difference between them is small—is clearly visible as a horizontal, dark blue region.

Results for the free-space measurement (i.e., with no cylinder), the bare dielectric cylinder, and the cloaked one were compared. The free-space measurement with no cylinder gave the picture of the incident field that impinged over the cylinder. The presence of the bare cylinder distorted the incident field, producing a reflection (i.e., standing wave) in the backward direction and shadow in the forward direction. It was expected that the scattered-field attenuation due to the cloak (Figure 12) would reduce its magnitude to one much smaller than that of the incident field for operating frequencies in the cloaking band (i.e., 3.39 GHz). The total field (i.e., incident plus scattered) was, therefore, similar to the incident one: the cloaked cylinder was nearly transparent and did not perturb the incident field. However, this cloaking effect should not be visible at other frequencies (i.e., 2.75 GHz), for which the incident field should be heavily distorted by the presence of the bare or cloaked cylinder.

In the free-space measurement, we observed the 2-D field distribution of the transmitting horn antenna (i.e., the incident field). The bare dielectric cylinder distorted the field in both Figures 15 and 16. As expected, the cloak partly restored the incident-field distribution at 3.39 GHz (i.e., the cloaking band) in Figure 15, but not at 2.75 GHz (i.e., far away from the cloaking band) in Figure 16.

To check the performance of forward near-field cloaking versus operating frequency, in Figure 17 we have integrated into the 2-D near-field grid the absolute value of the difference between the free space and the bare or cloaked-cylinder near-field magnitudes. Since the cloaked-cylinder near field

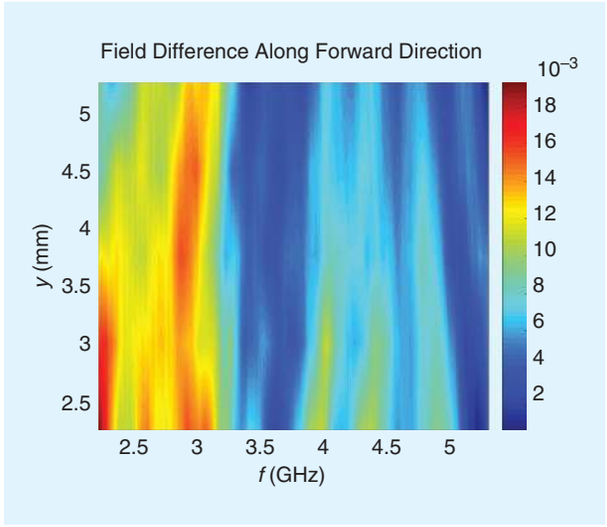

FIGURE 20. The absolute value of the difference between the free-space and the cloaked-cylinder field magnitudes along the forward *y*-direction (i.e., the center column of the 2-D measurement grid) versus the frequency. The cloaking band between 3.4 and 3.7 GHz—in which the incident and the cloaked-cylinder fields are similar so that the difference between them is small—is clearly visible as a vertical, dark blue region.

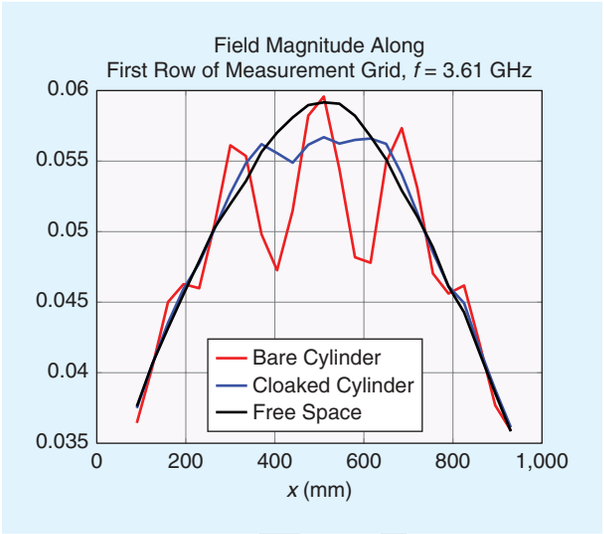

FIGURE 21. The near-field magnitude along the first row (i.e., the *x*-direction) of the 2-D measurement grid, for the free-space measurement (i.e., the incident field, with no cylinder) and the bare dielectric and cloaked cylinder at the frequency of best near-field restoration (i.e., 3.61 GHz). The near field is distorted by the presence of the bare cylinder, while the scattering cancelation due to the cloak produces a cloaked-cylinder field close to the incident one.

was similar to the incident one for operating frequencies in the cloaking band, we observed that the difference between them was, indeed, much smaller in the cloaking band than outside. This effect was not visible for the bare-cylinder near field.

Figure 17 shows a result similar to that of the bistatic scattering measurement in Figure 12, but the forward near-field cloaking band was between 3.4 and 3.7 GHz, while in Figure 12 the maximum attenuation of far-field scattering was between 3.3 and 3.4 GHz. Figure 18 shows the forward near field for the free-space and bare- and cloaked-cylinder measurements at the frequency of 3.61 GHz, for which the cloak best restored the incident field. Again, the total field distribution was heavily distorted by the presence of the bare cylinder, while the near field with cloak resembled the unperturbed incident field (i.e., the free-space measurement, without the cylinder), as expected.

It is remarkable that, according to Figure 4, in the band between 3.4 and 3.7 GHz, the surface impedance of the cylindrical FSS was close to the value of 192.5 Ω, which theoretically canceled the scattered field at 3.77 GHz. To display the similarity between the free space and the cloaked-cylinder near-field magnitudes versus operating frequency, Figures 19 and 20 show two cuts of the difference between the two field magnitudes; Figure 19 shows a horizontal cut in the *x*-direction along the first row of the 2-D measurement grid, while Figure 20 shows a vertical cut along the forward *y*-direction, which is the center column of the 2-D measurement grid.

The cloaking band between 3.4 and 3.7 GHz, in which the incident and cloaked-cylinder fields were similar so that the difference between them was small, is visible as a dark blue, horizontal region in Figure 19 and a vertical region in Figure 20.

Figure 21 displays the near-field magnitude along the first row (i.e., the *x*-direction) of the 2-D measurement grid for the three measurements—free space (i.e., with no cylinder), bare, and cloaked cylinders—at the frequency of best incident-field restoration (i.e., 3.61 GHz). As expected, the near field was distorted by the presence of the bare cylinder, and the scattering cancelation due to the cloak produced a cloaked-cylinder field close to the incident one.

CONCLUSIONS

A full process for the design, simulation, prototyping, and measurement of a simple and effective FSS-based mantle cloak for electrically small dielectric cylinders at 3.77 GHz has been presented. Full-wave 3-D simulations showed excellent agreement with theory. An original approach has been introduced to compute the effective surface impedance of the cylindrical metasurface, from either measured or simulated far fields.

Experimental prototype measurements showed about 10-dB scattered-field attenuation at a relatively broad band of 100 MHz at 3.4 GHz, although the scattering cancelation technique was theoretically narrow-band. Near-field measurements in the forward direction demonstrated that the cloak partly restored the incident field in a wider band between 3.4 and 3.7 GHz.

AUTHOR INFORMATION

Pedro Yuste (pyustega@gmail.com) is a consultant in the telecommunications field. **<AU: Please note that bios have been trimmed in accordance to magazine style. Please provide the author's current affiliation and research interests.>**

Juan M. Rius (rius@tsc.upc.edu) is a professor at the

CommSensLab, Universitat Politècnica de Catalunya–BarcelonaTech, Spain. His research interests include developing efficient algorithms for numerical analysis of electrically large antennas and scatterers, using either high-frequency approximations or integral equations.

Jordi Romeu (romeu@tsc.upc.edu) is a professor at the CommSensLab, Universitat Politècnica de Catalunya–BarcelonaTech, Spain. His research interests include antennas, electromagnetic scattering and imaging, and system miniaturization for wireless and sensing industrial and bio applications.

Sebastián Blanch (blanch@tsc.upcedu) is an associate professor at the CommSensLab, Universitat Politècnica de Catalunya–BarcelonaTech, Spain. His research interests include antenna near-field measurements, antenna diagnostics, and antenna design.

Alexander Heldring (heldring@tsc.upc.edu) is an associate professor at the CommSensLab, Universitat Politècnica de Catalunya–BarcelonaTech, Spain. His research interests include integral equation methods for electromagnetic problems and wire antenna analysis.

Eduard Ubeda (ubeda@tsc.upc.edu) is an associate professor at the CommSensLab, Universitat Politècnica de Catalunya–BarcelonaTech, Spain. His research interests include numerical computation of scattering and radiation using integral equations.

REFERENCES

[1] A. Alù and N. Engheta, "Achieving transparency with plasmonic and metamaterial coatings," *Phys. Rev. E.*, vol. 72, p. 016,623, July 2005. **<AU: Please check that the page number is correct.>**

[2] A. Alù and N. Engheta, "Multifrequency optical invisibility cloak with layered plasmonic shells," *Phys. Rev. Lett.*, vol. 100, Mar. 2008. **<AU: Please provide page range.>**

[3] J. B. Pendry, D. Schurig, and D. R. Smith, "Controlling electromagnetic fields," *Sci.*, vol. 312, no. 5781, pp. 1780–1782, June 2006.

[4] C. Caloz and T. Itoh, *Electromagnetic Metamaterials: Transmission Line Theory and Microwave Applications*. Hoboken, NJ: Wiley, 2005.

[5] G. V. Eleftheriades and K. G. Balmain, Eds., *Negative-Refraction Metamaterials*. Hoboken, NJ: Wiley, 2005.

[6] D. Schurig, J. J. Mock, B. J. Justice, S. A. Cummer, J. B. Pendry, A. F. Starr, and D. R. Smith, "Metamaterial electromagnetic cloak at microwave frequencies," *Sci.*, vol. 314, no. 5801, pp. 977–980, Nov. 2006.

[7] B. Edwards, A. Alù, M. G. Silveirinha, and N. Engheta, "Experimental verification of plasmonic cloaking at microwave frequencies with metamaterials," *Phys. Rev. Lett.*, vol. 103, Oct. 2009. **<AU: Please provide page range.>**

[8] B. I. Popa and S. A. Cummer, "Cloaking with optimized homogeneous anisotropic layers," *Phys. Rev. A*, vol. 79, no. 2, 2009. **<AU: Please provide page range.>**

[9] J. Andkjr and O. Sigmund, "Topology optimized low-contrast all-dielecteric optical cloak," *Appl. Phys. Lett.*, vol. 98, no. 2, 2011. **<AU: Please provide page range.>**

[10] X. Wang and E. Semouchkina, "A route for efficient non-resonance cloaking by using multilayer dielectric coating," *Appl. Phys. Lett.*, vol. 102, no. 11, 2013. **<AU: Please provide page range.>**

[11] L. S. Kalantari and M. H. Bakr, "Wideband cloaking of objects with arbitrary shape exploiting adjoint sensitivities," *IEEE Trans. Antennas and Propag.*, vol. 64, no. 5, May 2016. **<AU: Please provide page range.>**

[12] B. A. Munk, *Frequency Selective Surfaces: Theory and Design*. New York: Wiley, 2000.

[13] A. Alù, "Mantle cloak: Invisibility induced by a surface," *Phys. Rev. B*, vol. 80, no. 24, Dec. 2009. **<AU: Please provide page range.>**

[14] P. Y. Chen and A. Alù, "Mantle cloaking using thin patterned metasurfaces," *Phys. Rev. B*, vol. 84, no. 20, Nov. 2011. **<AU: Please provide page range.>**

[15] P. Y. Chen, J. Soric, and A. Alù, "Invisibility and cloaking based on scattering cancelation," *Advanced Materials*, vol. 64, no. 44, pp. 281–304, Nov. 2012.

[16] P. S. Kildal, A. A. Kishk, and A. Tengs, "Reduction of forward scattering from cylindrical objects using hard surfaces," *IEEE Trans. Antennas Propag.*, vol. 44, no. 11, Nov. 1996. **<AU: Please provide page range.>**

[17] P. S. Kildal, "Artificially soft and hard surfaces in electromagnetics," *IEEE Trans. Antennas Propag.*, vol. 38, no. 10, pp. 1537–1544, Oct. 1990.

[18] M. Riel, Y. Brand, Y. Demers, and P. de Maagt, "Performance improvements of center-fed reflector antennas using low scattering struts," *IEEE Trans. Antennas Propag.*, vol. 60, no. 3, Mar. 2012. **<AU: Please provide page range.>**

[19] J. C. Soric, P. Y. Chen, A. Kerkhoff, D. Rainwater, K. Melin, and A. Alù, "Demonstration of an ultralow profile cloak for scattering suppression of a finite-length rod in free space," *New J. Phys.*, vol. 15, 2013. **<AU: Please provide the issue number or month and the page range.>**

[20] P. Y. Chen, F. Monticone, and A. Alu, "Suppressing the electromagnetic scattering with an helical mantle cloak," *IEEE Antennas Wireless Propag. Lett.*, vol. 10, pp. 1598–1601, 2011. **<AU: Please provide the issue number or month.>**

[21] A. Monti, J. Soric, A. Alu, F. Bilotti, A. Toscano, and L. Vegni, "Overcoming mutual blockage between neighboring dipole antennas using a low-profile patterned metasurface," *IEEE Antennas Wireless Propag. Lett.*, vol. 11, pp. 1414–1417, 2012. **<AU: Please provide the issue number or month.>**

[22] J. C. Soric, A. Monti, A. Toscano, F. Bilotti, and A. Al, "Dual-polarized reduction of dipole antenna blockage using mantle cloaks," in *IEEE Trans. Antennas Propag.*, vol. 63, no. 11, pp. 4827–4834, Nov. 2015.

[23] A. Monti, J. Soric, A. Alù, A. Toscano, and F. Bilotti, "Anisotropic mantle cloaks for TM and TE scattering reduction," *IEEE Trans. Antennas Propag.*, vol. 63, no. 4, p. 1775, Apr. 2015. **<AU: Please check that the page number is correct.>**

[24] P. Yuste, J. M. Rius, J. Romeu, S. Blanch, A. Heldring, and E. Ubeda, "A simple and effective microwave invisibility cloak based on frequency selective surfaces," in *Proc. 11th European Conf. Antennas and Propagation (EuCAP)*, Paris, France, Mar. 2017. **<AU: Please provide the page range.>**

[25] C. A. Balanis, "Appendix IV" in *Advanced Engineering Electromagnetics*. New York: Wiley, 1989.

[26] J. Baker-Jarvis, E. J. Vanzura, and W. A. Kissick, "Improved technique for determining complex permittivity with the transmission/reflection method," *IEEE Trans. Microw. Theory Techn.*, vol. 38, no. 8, pp. 1096–1103, Aug. 1990.

[27] Y. R. Padooru, A. B. Yakolev, P. Y. Chen, and A. Alù, "Analytical modeling of conformal mantle cloaks for cylindrical object using sub-wavelength printed and slotted arrays," *J. Appl. Phys.*, vol. 112, 2012. **<AU: Please provide the issue number or month and the page range.>**

[28] S. Rao, D. Wilton, and A. Glisson, "Electromagnetic scattering by surfaces of arbitrary shape," *IEEE Trans. Antennas Propag.*, vol. 30, no. 3, pp. 409–418, May 1982.

[29] D. Schaubert, D. Wilton, and A. Glisson, "A tetrahedral modeling method for electromagnetic scattering by arbitrarily shaped inhomogeneous dielectric bodies," *IEEE Trans. Antennas Propag.*, vol. 32, no. 1, pp. 77–85, Jan. 1984.

[30] C. C. Lu and W. C. Chew, "A coupled surface-volume integral equation approach for the calculation of electromagnetic scattering from composite metallic and material targets," *IEEE Trans. Antennas Propag.*, vol. 48, no. 12, pp. 1866–1868, Dec. 2000.

[31] N. Morita, N. Kumagai, and J. R. Mautz, *Integral Equation Methods for Electromagnetics*. Norwood, MA: Artech House, 1990.

[32] R. F. Harrington, *Field Computation by Moment Methods*. New York: Macmillan, 1968.

[33] J. M. Rius, J. Parrón, A. Heldring, J. M. Tamayo, and E. Ubeda, "Fast iterative solution of integral equations with method of moments and matrix decomposition algorithm singular value decomposition," *IEEE Trans. Antennas and Propag.*, vol. 56, no. 8, pp. 2314–2324, Aug. 2008.

[34] C. A. Balanis, *Advanced Engineering Electromagnetics*. New York: Wiley, 1989.

[35] Dassault Systemes. Computer simulation technology. [Online]. Available: http://www.cst.com/ **<AU: Please provide the year or date of access if possible.>**

An FSS is probably the most cost-effective and easiest-to-implement choice for putting scattering cancelation into practice.

The aim of this article is to didactically present the complete process.

The magnetic field inside and outside the cylinder was obtained from the electric field (7) and (8) after applying Maxwell-Faraday curl equation.

This result gave the surface reactance of the cloaking coat attached to an electrically thin cylinder that minimized the scattered field and, thus, reduced its visibility.

The cloak is expected to work successfully at a frequency of 3.78 instead of 3.77 GHz.

The incident and cloaked-cylinder fields were similar so that the difference between them was small.

The bending of the FSS in a curved surface did not significantly change the surface impedance near 3.77 GHz.

The total field distribution was heavily distorted by the presence of the bare cylinder.